ORIGINAL PAPER

Acetone sensor based on solvothermally prepared ZnO doped with Co$_3$O$_4$ nanorods

**Mohammed M. Rahman · Sher Bahadar Khan ·
Abdullah M. Asiri · Khalid A. Alamry ·
Aftab Aslam Parwaz Khan · Anish Khan ·
Malik Abdul Rub · Naved Azum**

Abstract This paper describes a reliable and sensitive method for sensing dissolved acetone using doped nanomaterials. Large-scale synthesis of ZnO nanorods (NRs) doped with Co$_3$O$_4$ was accomplished by a solvothermal method at low temperature. The doped NRs were characterized in terms of their morphological, structural, and optical properties by using field-emission scanning electron microscopy coupled with energy-dispersive system, UV-Vis., Fourier transform IR, X-ray diffraction, and X-ray photoelectron spectroscopy. The calcinated (at 400 °C) doped NRs are shown to be an attractive semiconductor nanomaterial for detecting acetone in aqueous solution using silver electrodes. The sensor exhibits excellent sensitivity, stability and reproducibility. The calibration plot is linear over a large concentration range (66.8 μM to 0.133 mM), displays high sensitivity (~3.58 μA cm^{-2} mM^{-1}) and a low detection limit (~14.7±0.2 μM; at SNR of 3).

Keywords ZnO doped Co$_3$O$_4$ nanorods · Solvothermal method · Acetone determination · I-V nanomaterials

M. M. Rahman · S. B. Khan · A. M. Asiri · K. A. Alamry ·
A. A. P. Khan · A. Khan · M. A. Rub · N. Azum
Center of Excellence for Advanced Materials Research (CEAMR),
King Abdulaziz University, Jeddah 21589,
P.O. Box 80203, Saudi Arabia

M. M. Rahman (✉) · S. B. Khan · A. M. Asiri · K. A. Alamry ·
A. A. P. Khan · A. Khan · M. A. Rub · N. Azum
Chemistry Department, Faculty of Science, King Abdulaziz
University, P. O. Box 80203, Jeddah 21589, Saudi Arabia
e-mail: mmrahman@kau.edu.sa

Introduction

Doped nanomaterial has been recognized as a promising host for transition material revealing a stable morphological structure and is composed of a number of irregular phases with geometrically coordinated metal and oxide atoms stacked alternately along the axes [1]. Transition metals doped-semiconductor nanomaterials have been used in insightful research efforts due to their exceptional optical and structural properties as well as versatile applications [2]. Recently, extensive developments have been made in the research leading to ZnO-based doped nanomaterials initiated by both fundamental sciences and advanced technologies [3]. This doped nanostructure material exhibits promising uses as field consequence transistors, UV photo-detectors, gas-sensors, field-emission electron sources, nanomaterials, nanoscale power generators, and many other functional devices [4–10]. Preparation of doped material is also a competent method to regulate the energy-level surface states of zinc oxide, which can further progress by changing the doping concentration of semiconductor materials. As one of the most interesting magnetic p-type doping materials, cobalt-oxide nanostructure is also recognized as an attractive material with broad applications in various fields, such as doping, catalysts, solid-state sensors, and electrochemical devices [11–13]. Undoped zinc oxide semiconductor material (band-gap~3.37 eV) is a substantial functional nanomaterial applied in various fields, such as solar cells, photocatalysis, optoelectronic, electrical, electromagnetic shielding, bio- and chemo-sensors [14]. It has gained much interest owing to proficient synthesis, easy handling, economical way of preparation, reproducibility and applications as a gas-sensor for the detection of toxic materials such as

hydrogen, ammonia, liquid petroleum gas, ethanol, formaldehyde, ammonium hydroxide, alcohols, and phenol [15, 16].

Semiconductor nanomaterials have attracted considerable interest owing to their extrinsic and remarkable properties in the electrical, optical, thermal, and mechanical fields as compared to their undoped materials. It is essential for the preparation of nanomaterials to achieve exceptional quality of doped semiconductor structures. To this end an extensive range of chemical and physical methods has been used for the preparation of Co_3O_4 nanomaterials, including polymer ignition, gel-technology, co-precipitation, ball-milling, chemical vapor deposition and others [17–21]. Co-doped nanomaterials uncovered several applications because of their attractive properties resulting from the changeable oxidation state of the transition-semiconductor metals. The impressive nano-structural morphology of transition metal oxides is the amendment of magnetic and electrical properties. It is well recognized that Co_3O_4 has an extraordinary nanostructure, and doped Co_3O_4 exhibits anti-ferromagnetism at lower temperatures [22]. In industries and research laboratories, highly volatile and toxic acetone is frequently used. It is harmful to human health and living organisms in health care and environmental fields. Exposure to air having high concentrations of acetone vapor may cause headache, allergy, fatigue, and even narcosis [23]. For diabetes mellitus patients, it is very harmful to inhale the toxic acetone, thus urgently requiring to investigate the sugar-level regularly [24]. Hence early detection and quantification of acetone in the environment is necessary and important for our safety in the research laboratory and industrial premises. Recently, metal oxides have been exploited as artificial mediators for the development of reliable and efficient chemo-sensors [25]. Therefore doped semiconductor materials have been utilized as a redox mediator for the detection and quantification of acetone using reliable electrochemical approaches at room temperature.

Doped metal oxides are also the model materials for sensing due to their highly active surface areas, and they are extensively employed as chemosensor for the detection, recognition, and quantification of various carcinogenic pollutants as well as toxic chemicals or biomolecules [26]. In the presence of organic volatile chemicals, acetone causes damage to the brain and specific diseases of the stomach, liver, and erythrocytes. Consequently it is a significant and big challenge to detect acetone proficiently and hence protect human health from insidious diseases and save the environment using analytical techniques [27]. A large amount of metal oxides have been considered as chemosensors for the detection of different hazardous pollutants and toxic chemicals [28, 29]. Therefore ZnO-doped Co_3O_4 NRs have been offered as mediator to detect and detoxify the organic acetone chemical. The main focus of this present investigation is to fabricate and develop a highly sensitive chemical sensor for the detection and

quantification of hazardous pollutants using NR semiconductor nanomaterials. Doped nanomaterials are extensively employed for the detection of hazardous molecules in chemical control process due to their numerous benefits over conventional chemical analysis in terms of response, large-surface area, portability, and monitoring of toxic chemical in the environmental field. Conventional electrochemical methods with uncoated nanomaterial electrodes for acetone detection exhibit a slower-response, surface-fouling, unstable signals, noise, and lower sensitivity. Hence, modification of the sensor surface with doped nanomaterials is very important to achieve more sensitive, repeatable, and stable responses. Therefore, a simple and reliable I-V electrochemical approach paired with relatively easy, convenient and inexpensive instrumentation is required to obtain higher sensitivity and lower detection limits compared to conventional methods. Here, we introduced a very reliable, large-scale, highly sensitive technique for the electrochemical detection of acetone using ZnO-doped Co_3O_4 NRs at room temperature. The present approach depicts a simple, highly sensitive, low-sample volume, easy to handle, and precise I-V technique.

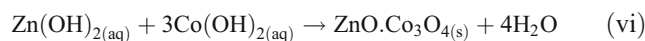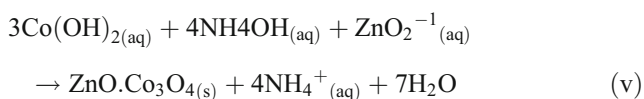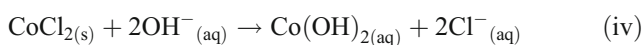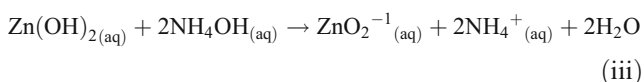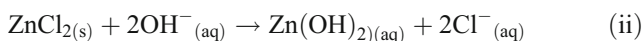## Experimental

Chemical reagents and apparatus

Zinc chloride ($ZnCl_2$), cobalt chloride ($CoCl_2$), ethyl acetate, disodium phosphate, butyl carbitol acetate, monosodium phosphate, and all the other chemicals used were of analytical grade and obtained from Sigma-Aldrich Company (http://www.sigmaaldrich.com). 0.1 M phosphate buffer solution at pH 7.0 was prepared by mixing equimolar concentrations of 0.2 M Na_2HPO_4 and 0.2 M NaH_2PO_4 solution in 100.0 mL deionized water at room temperature. The λ_{max} (397.0 nm) of ZnO-doped Co_3O_4 nanorods was evaluated with UV/visible spectroscopy (UV/Vis., Lamda-950, Perkin Elmer, Germany; http://www.perkinelmer.com). Fourier-transform infrared spectroscopy (FT-IR spectra) was performed with a spectrophotometer (Spectrum-100 FT-IR) in the mid-IR range, which was purchased from Perkin Elmer, Germany (http://www.perkinelmer.com). A Raman station 400 (Perkin Elmer, Germany; http://www.perkinelmer.com) was used to measure the Raman shift of doped nanorod materials using radiation source (Ar^+ laser line, λ; 513.4 nm). The powder X-ray diffraction (XRD) prototypes were assessed with an X-ray diffractometer (XRD; X'Pert Explorer, PANalytical diffractometer; www.panalytical.com) equipped with Cu-$K_{\alpha1}$ radiation ($\lambda = 1.5406$ nm) using a generator voltage of 40.0 kV and a generator current of 35.0 mA applied for the purpose. The XPS measurements were executed on a Thermo Scientific K-Alpha KA1066 spectrometer (Germany). Monochromatic Al$K\alpha$ x-ray radiation sources were used as excitation sources,

where the beam-spot size was kept at 300.0 μm. The spectra were recorded in the fixed analyzer transmission mode, where the pass energy was kept at 200 eV. Scanning of the spectra was performed at lower pressures ($<10^{-8}$ Torr). The morphology of doped nanomaterial was investigated by field-emission scanning electron microscopy (FESEM; JSM-7600F, Japan; www.jeol.com). I-V technique was used for the investigation of acetone using an Electrometer (Kethley, 6517A, Electrometer, USA; www.keithley.com) at room temperature.

Synthesis and growth mechanism of ZnO-doped Co₃O₄ NRs

Initially, cobalt chloride (0.1 M) and zinc chloride (0.1 M) solution were prepared separately with de-ionized water at room temperature. The equimolar solution of both reactants was mixed gently at 1:1 ratio. Then the reducing agent (i.e., NH₄OH) was added dropwise into the reactant mixture to produce a white precipitate. The resultant solution was adjusted to pH~10.15 using NH₄OH solution. The mixture was transferred into a hydrothermal cell (Teflon autoclave) and placed in the oven at a temperature of about 150.0 °C for 16 h (active solution temperature, ~92.0 °C). Then the solution was left for cooling down to room temperature for several hours. The precipitate was separated and consecutively washed thoroughly with ethanol, acetone and water. Finally, the grown ZnO-doped Co₃O₄ NRs were placed for calcinations into the furnace at 400.0 °C for 5 h (Barnstead Thermolyne, 6000 Furnace, USA). The calcinated products were characterized in detail in terms of their morphological, structural, optical properties, and applied for acetone drug detection.

The growth mechanism of the doped nanomaterials could be explained on the basis of chemical reaction and nucleation as well as the development of host nanocrystals. The apparent reaction mechanism leading to the doped nanomaterials is anticipated as follows:

$$NH_4OH_{(aq)} \rightarrow NH_4^+{}_{(aq)} + OH^-{}_{(aq)} \tag{i}$$

$$ZnCl_{2(s)} + 2OH^-{}_{(aq)} \rightarrow Zn(OH)_{2(aq)} + 2Cl^-{}_{(aq)} \tag{ii}$$

$$Zn(OH)_{2(aq)} + 2NH_4OH_{(aq)} \rightarrow ZnO_2^{-1}{}_{(aq)} + 2NH_4^+{}_{(aq)} + 2H_2O \tag{iii}$$

$$CoCl_{2(s)} + 2OH^-{}_{(aq)} \rightarrow Co(OH)_{2(aq)} + 2Cl^-{}_{(aq)} \tag{iv}$$

$$3Co(OH)_{2(aq)} + 4NH4OH_{(aq)} + ZnO_2^{-1}{}_{(aq)}$$
$$\rightarrow ZnO.Co_3O_{4(s)} + 4NH_4^+{}_{(aq)} + 7H_2O \tag{v}$$

$$Zn(OH)_{2(aq)} + 3Co(OH)_{2(aq)} \rightarrow ZnO.Co_3O_{4(s)} + 4H_2O \tag{vi}$$

The precursors of CoCl₂ and ZnCl₂ are reacted in the alkaline medium according to the Eqs. (i) to (iv). After addition of reducing agent (NH₄OH) into the mixture of reactant solution, the reaction is slowly progressed to growth the co-doped nanomaterials according to the Eqs. (v)–(vi). During the total synthesis process, NH₄OH acts as a pH buffer to regulate the pH value of the solution and slow release of OH⁻ ions [30]. When the concentration of Zn²⁺ and OH⁻ ions exceeded a critical value, the precipitation of ZnO nuclei begins to start. As there is a high concentration of Co²⁺ ions in the reaction medium, the nucleation of ZnO crystals is also started to co-precipitate, owing to the lower activation energy barrier of heterogeneous nucleation. However, due to the low concentration of Co²⁺ ions in the reaction medium, the larger ZnO crystals with a rod-like morphology are developed among the nanostructures composed of ZnO co-doped Co₃O₄ NRs. The shape of the NRs is approximately consistent with the growth habit of transition-metal doped ZnO crystals [31, 32].

Fabrication of the sensor and detection technique for acetone

The silver electrode (AgE) is prepared with ZnO-doped Co₃O₄ NRs, where butyl carbitol acetate (BCA) and ethyl acetate (EA) act as conducting binders. A small amount (0.1 μg each) of mixture (EA, BCA, and ZnO-doped Co₃O₄) is uniformly pasted onto the AgE surfaces, and then placed into the oven at 70.0 °C for 12 h until the film is completely dry. An electrochemical cell is mounted with doped nanomaterials coated AgE as a working electrode and Pd wire is used as counter-electrode. Stock solution of acetone (1.33 M) is diluted to various concentrations and used as a target. An amount of 0.1 M phosphate buffer solution is kept constant in the beaker as 10.0 mL throughout the chemical investigation. The acetone analyte solution is made with various concentrations in the range of 66.8 μM to 1.33 M. The sensitivity is calculated from the slope of current vs. concentration (I vs. C) from the calibration plot divided by the value of active-surface area of fabricated AgE electrodes. An electrometer is used as a voltage source for I-V technique in two electrode systems.

Results and discussion

Investigation of optical properties

The optical property of the ZnO-doped Co3O4NRs is one of the significant characteristics for the assessment of its photo-catalytic activity. The optical absorption spectra of ZnO co-

doped Co_3O_4 NRs are measured by using a UV-Vis spectrophotometer in the visible range (200.0 to 800.0 nm). UV/visible absorption is a technique in which the outer electrons of atoms or molecules absorb radiant energy and undergo transitions to high energy levels. In this phenomenon, the spectrum obtained due to optical absorption can be analyzed to acquire the energy band gap of the semiconductor. The optical absorption measurement was carried out at ambient conditions. From the absorption spectrum, the absorbance of the ZnO-doped Co_3O_4 NRs was measured and found to be about 397.0 nm, as shown in Fig. 1a. The band gap energy (E_{bg}) is calculated on the basis of the maximum absorption band of NRs and was found to be 3.1234 eV, according to the following Eq. (vii).

$$E_{bg} = \frac{1240}{\lambda} \, (ev) \tag{vii}$$

where E_{bg} is the band-gap energy, and λ_{max} is the wavelength (397.0 nm) of the NRs. No extra peak associated with impurities and structural defects were observed in the spectrums, which proved that the synthesized NRs control the crystallinity of ZnO-doped Co_3O_4 nanomaterials [33].

The ZnO-doped Co_3O_4 NRs were also studied in terms of atomic and molecular vibrations. To predict the motivated identification, FT-IR spectra with fundamental absorption in the range of 400–4,000 cm^{-1} are investigated at room temperature. Figure 1b displays the FT-IR spectrum of the ZnO-doped Co_3O_4 nanostructures. It represents bands at 668, 1,243, 1,600, and 3,446 cm^{-1}. This broad vibration band (at 668 cm^{-1}) could be assigned to metal-oxygen (Co–O and Zn–O modes) stretching vibrations [34], which demonstrated the configuration of doped nanostructure materials. The supplementary vibrational bands may be assigned to O–H bending vibration (1,600 cm^{-1}), C–O absorption (1,243 cm^{-1}), and O–H stretching (3,446 cm^{-1}). The absorption bands at 1,243, 1,600, and 3,446 cm^{-1} usually results from CO_2 and water, which due to their high surface-to-volume ratio of mesoporous nature are absorbed by semiconductor nanostructure materials from the environment [35]. Finally, the experimental vibration bands in low frequency regions suggested the formation of ZnO-doped Co_3O_4 NRs.

Raman spectroscopy is a spectroscopic technique used to disclose vibrational, rotational, and other low-frequency phases in Raman active compounds. It is based on inelastic scattering of monochromatic light (called Raman scattering), usually from a laser in the visible, near-infrared, or near-ultraviolet range. The laser light interacts with molecular vibrations, which caused an upward or downward shift of

Fig. 1 Typical **a** UV–vis spectrum, **b** FTIR spectrum, and **c** Raman spectrum of ZnO-doped Co_3O_4 NRs
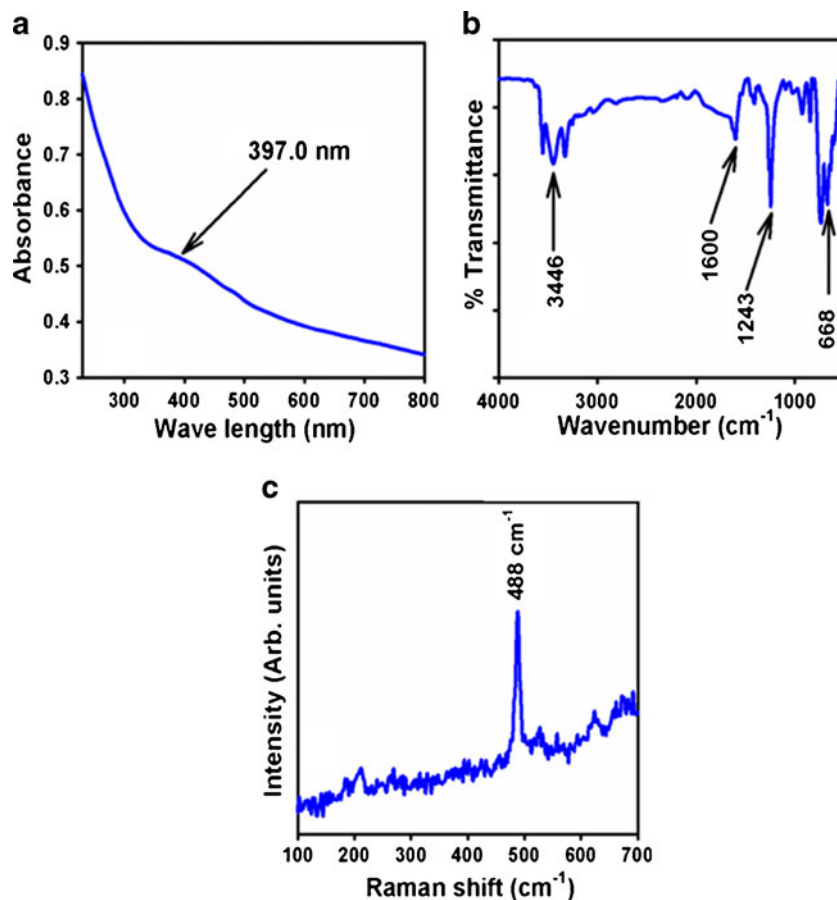
the energy of the laser photons. Raman spectroscopy is usually recognized and utilized in material chemistry, since the information is explicit to the chemical bonds and symmetry of metal–oxygen stretching or vibrational modes. Figure 1c confirms the Raman spectrum where key aspects of the wave number are measured at 488 cm^{-1} for metal–oxygen (Co–O and Zn–O) stretching vibrations. These bands can be assigned to a cubic phase of ZnO-doped Co$_3$O$_4$ NRs [36].

Investigation of morphological, elemental, and structural properties

High resolution FESEM images of ZnO-doped Co$_3$O$_4$ NRs are shown in Fig. 2a to c (magnified). The images are composed of nanostructure materials with aggregated nanostructure in rod shapes. The average diameter is calculated in the range of 35.15 nm to 51.23 nm, which is close to 42.98±5.0 nm. It is shown clearly from the FESEM images

that the simple hydrothermal methodology of synthesized doped products creates the nanostructure of ZnO-co-doped Co$_3$O$_4$, which flourished to form an extraordinarily rod-shape of high-density.

The crystallinity and crystal phases of the ZnO-doped Co$_3$O$_4$ NRs were examined. The X-ray diffraction patterns of doped NRs are shown in Fig. 2. The ZnO-doped Co$_3$O$_4$ NRs were investigated and shown as face-centered cubic. The as-grown sample was heated in a furnace at 400.0 °C to start the formation of nano-crystalline doped phases. Figure 2d reveals characteristic crystallinity of the combined ZnO-doped Co$_3$O$_4$ NRs and their aggregative crystal arrangement. The reflection peaks in this prototype were initiated to correspond with the Co$_3$O$_4$ phase (star symbol, *) having face-centered-cubic geometry [Joint Committee on Powder Diffraction Standards (JCPDS) # 078-1970]. The phases demonstrated the key feature peaks (blue-color with *) with indices for crystalline Co$_3$O$_4$ at 2θ values of 31.27(220), 38.

Fig. 2 a–c low to high magnified FE-SEM images, d powder X-ray diffraction pattern, and e EDS investigation of ZnO-doped Co$_3$O$_4$ NRs

Element	Weight%	Atomic%
O K	26.14	74.98
Zn K	2.21	1.55
Co L	71.65	23.47
Totals	100.00	
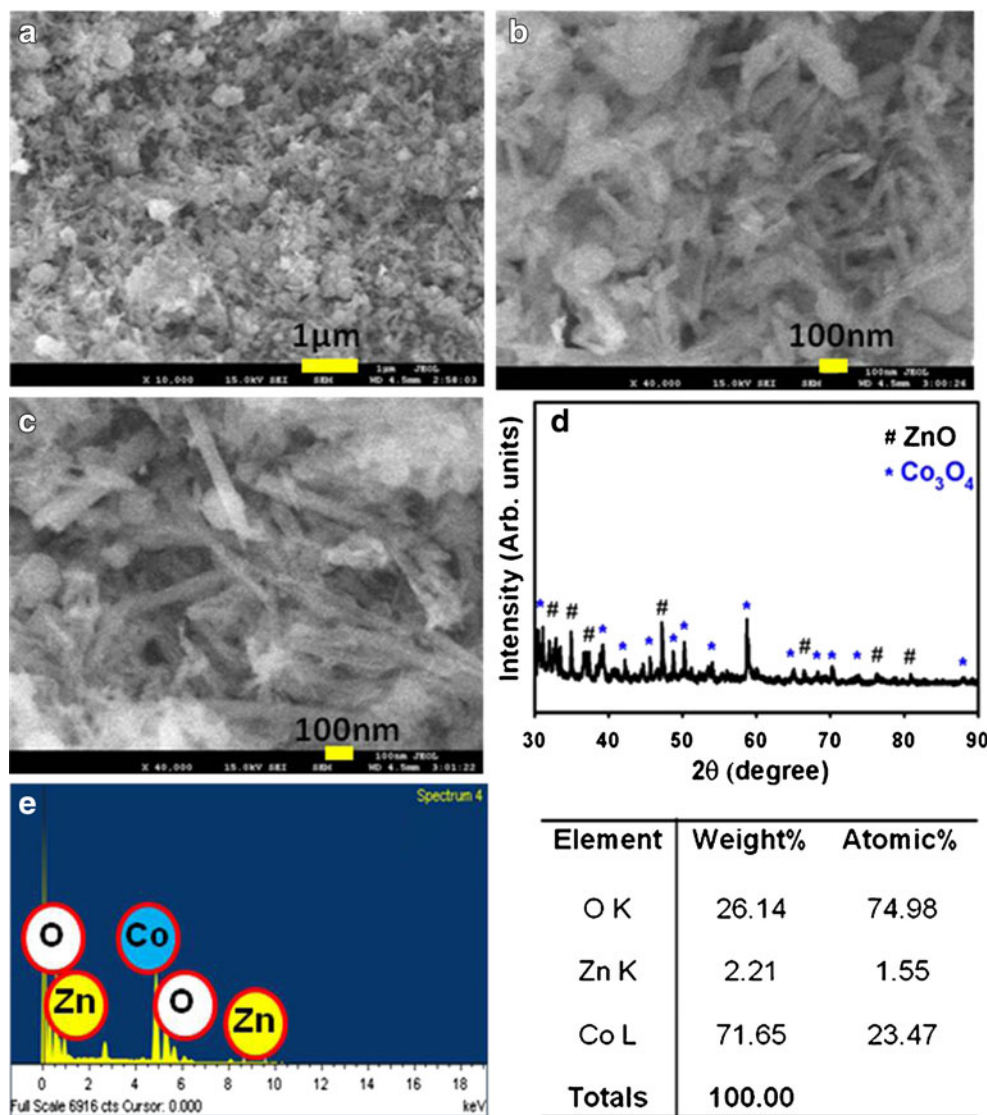
54(222), 44.80(400), 49.08(331), 55.65(422), 59.35(511), 65.22(440), 68.62(531), and 74.11(620) degrees. The face-centered-cubic lattice parameters are (a, 8.085), point group (Fd-3m), and radiation (CuK$_\alpha$1, λ=1.5406). This confirmed that there is a major number and amount of crystalline Co_3O_4 present in doped nanomaterials. Beside this, all the reflection peaks in this pattern were also found to match with the ZnO phase (Zincite) having hexagonal geometry [JCPDS # 074-9942]. The phases showed the major characteristic peaks (black-color, hash symbol, #) with indices for crystalline ZnO at 2θ values of 35.01(002), 36.8(101), 48.32(102), 67.43(200), 78.3(202), and 82.99(104) degrees. The hexagonal (unit cell) lattice parameters are a=3.2049; c=5.1216; Z=2, point group: P63mc (186), and radiation: CuK$_\alpha$1 (λ=1.5406). These indicate that there is a considerable amount of crystalline ZnO present in doped nanostructured materials. Finally, this x-ray pattern corresponds to the ZnO-doped Co_3O_4 NRs sample, which may be attributed to the doping of Co_3O_4 and the ZnO lattice site of doped aggregated NRs semiconductor materials [37]. Furthermore, no other impurity peak was observed in the XRD pattern showing the ZnO-doped Co_3O_4 phase formation. The electron dispersive spectroscopy (EDS) investigation of ZnO-doped Co_3O_4 NRs indicates the presence of Zn, Co, and O composition in the pure doped material. It is clearly shown that synthesized materials controlled only zinc, cobalt, and oxygen elements, which are presented in Fig. 2e. The composition of zinc, cobalt, and oxygen is 2.21 %, 71.65 %, and 26.14 %, respectively. No other peak related with any impurity has been detected in the EDS, which confirms that the doped products are composed only with zinc, cobalt, and oxygen.

X-ray photoelectron spectroscopy (XPS) is a quantitative spectroscopic method that determines the chemical-states of the elements that are present within co-doped materials. XPS spectra are acquired by irradiating on a nanomaterial with a beam of X-rays, while simultaneously determining the kinetic energy and number of electrons that get away from the top one to ten nm of the material being analyzed. Here, XPS measurements were measured for ZnO-doped Co_3O_4 NRs to investigate the chemical states of Co_3O_4 and ZnO. The XPS spectra of Co2p, Zn2p, and O1s are presented in Fig. 3a. Figure 3b presents the XPS spectra (spin orbit doublet peaks) of the Co2p$_{(3/2)}$ and Co2p$_{(1/2)}$ regions recorded with semiconductor co-doped nanomaterials. The binding energy of the Co2p$_{(3/2)}$ and Co2p$_{(1/2)}$ peak at 788.3. eV and 804.7 eV respectively denotes the presence of Co_3O_4 since their binding energies are similar to the reported work [38]. In Fig. 3c, the spin orbit peaks of the Zn2p$_{(3/2)}$ and Zn2p$_{(1/2)}$ binding energy for co-doped nanomaterials appeared at around 1050.8 eV and 1028.2 eV respectively, which is in good agreement with the reference data for ZnO [39]. The O1s spectrum shows a main peak at 532.1 eV in Fig. 3d. The peak at 532.1 eV is assigned to lattice oxygen may indicate oxygen

(i.e., O_2^-) presence in the co-doped nanomaterials [40]. XPS compositional analyses confirmed the co-existence of the two single-phases of Co_3O_4 and ZnO materials. Therefore, it is concluded that the solvothermally prepared Co_3O_4-ZnO materials have NRs phase contained two different materials. This conclusion is supported by XRD data (see Fig. 3).

Detection of acetone using I-V technique

Due to their mechanical strength, good conductivity, large surface area, and extremely miniaturized size of ZnO-doped Co_3O_4 NRs have been widely employed in electrode modification and toxic chemical detection. The doped NRs were applied for the detection of acetone in a liquid phase system at room temperature. Initially, the thin-film was fabricated using conducting binder (BCA/EA) and embedded on the AgE. The fabrication process and detection techniques are presented in the schematic diagram (Scheme 1). The PdE and NRs doped AgE were used as counter-electrode and working electrodes respectively, as presented in Scheme 1a and b respectively. The acetone was used as a target chemical in the liquid phase. The electrical responses in the presence of the toxic chemical were measured using I-V method according to Scheme 1c. The physic-sorption behaviors (adsorption and absorption) as well as the detection mechanism of ZnO-doped Co_3O_4 NRs are presented in Scheme 1d. Here the acetone molecules are absorbed as well as adsorbed onto the fabricated surfaces in huge amounts due to their mesoporous nature and the large active surface area of nanostructure material in liquid phase respectively.

Figure 4a displays the current responses of the uncoated (gray-dotted) and coated (dark-dotted) AgE working electrode (surface area, 0.0216 cm^2) with ZnO-doped Co_3O_4 NRs at room temperature. With the NRs fabricated surface, the current signal is reduced compared to NRs without fabricated surface, which reveals that the surface is slightly blocked with doped nanomaterials. The current changes for the doped nanomaterials modified electrodes before (dark-dotted) and after (blue-dotted) injecting 50.0 μL acetone (66.8 μM) in 10.0 mL phosphate buffer solution is presented in Fig. 4b. These considerable changes of surface current are measured with every injection of the target acetone into the electrochemical solution using an electrometer. 10.0 mL of 0.1 M phosphate buffer solution is originally transferred into the cell and the low to high concentration of acetone is added drop-wise consecutively from the stock solution. I-V responses with the ZnO-doped Co_3O_4 NRs modified electrode surface are evaluated from the different concentrations (66.8 μM to 1.33 M), as shown in Fig. 4c. It shows the current changes of fabricated films as a function of acetone concentration at room temperature. It is also observed that with increasing concentration of acetone, the resultant currents also increase significantly, which confirms

Fig. 3 XPS of calcined **a** doped ZnO-doped Co_3O_4 NRs, **b** Co2p, **c** Zn2p level, and **d** O1s level acquired with MgKα radiations
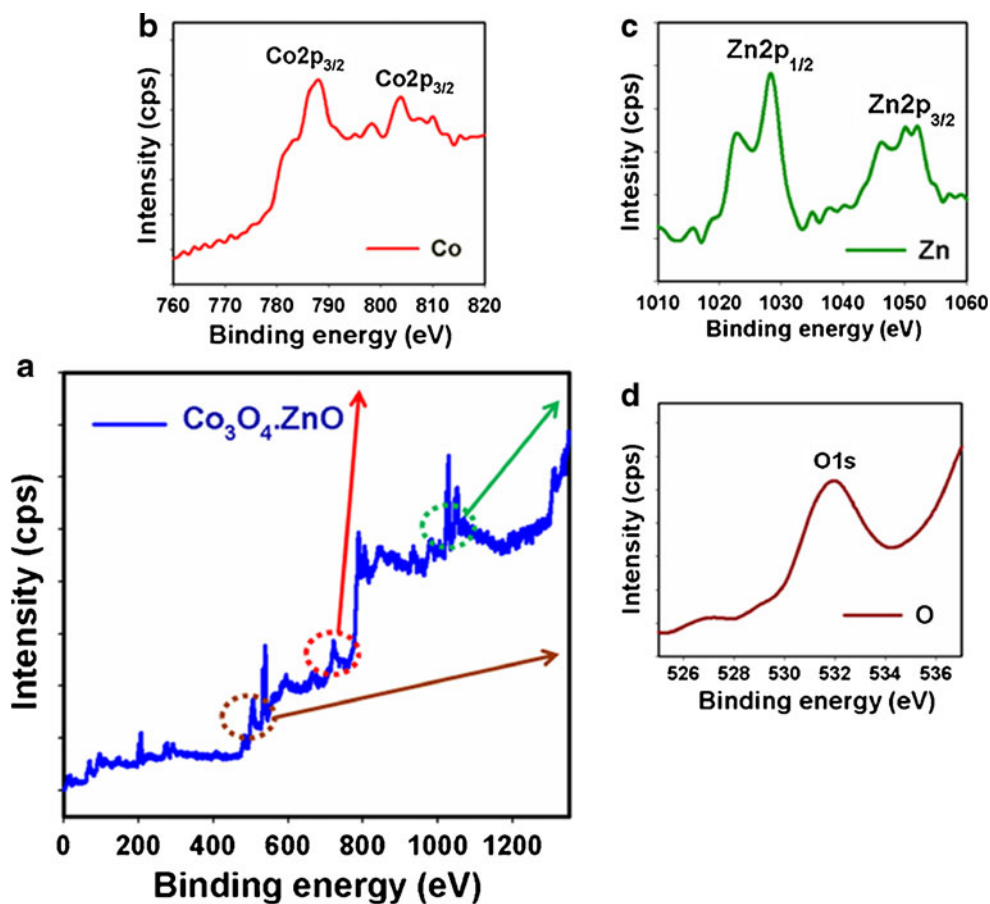
that the response is a surface process. It shows the response of doped NRs as a function of acetone concentration at room temperature. A large range of acetone concentrations is selected to study the probable analytical parameters, which are calculated in 66.8 μM to 1.33 M. The calibration curve was plotted from the variation of acetone concentrations

(at +0.7 V), which is presented in Fig. 4d. It exhibits a calibration curve for the response current versus acetone concentration of fabricated ZnO-doped Co_3O_4 NRs on the AgE sensor. It is observed from the calibration curve that, as the concentration of acetone increases, the current response also increases, and finally at a high-acetone concentration,

Scheme 1 Fabrication process and methodology of acetone sensors using ZnO-doped Co_3O_4 nanorods
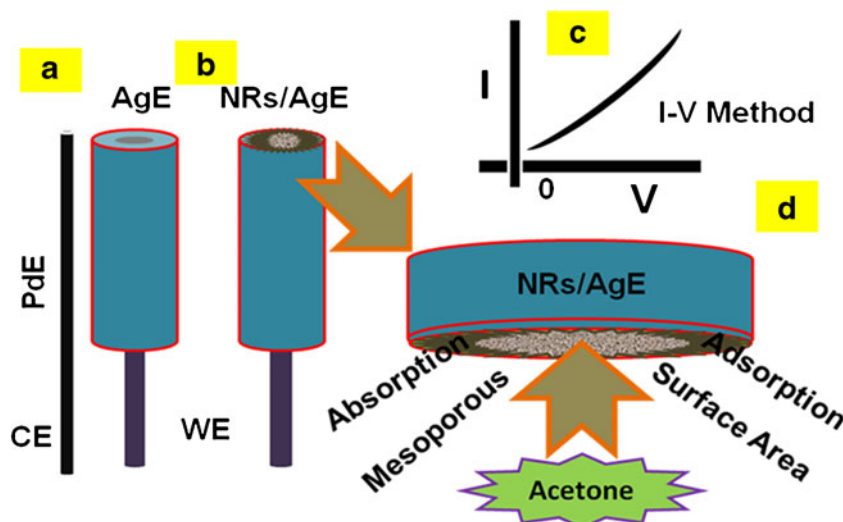
Fig. 4 I-V responses of **a** un-
coated and coated AgE; **b**
without and with acetone
(66.8 μM) in 10.0 mL
phosphate buffer solution;
c concentration variations
(66.8 μM to 1.33 M) of
acetone; **d** calibration plot
(at +0.7 V), and **e** repeatability
signals of ZnO-doped Co_3O_4
NRs fabricated on AgE
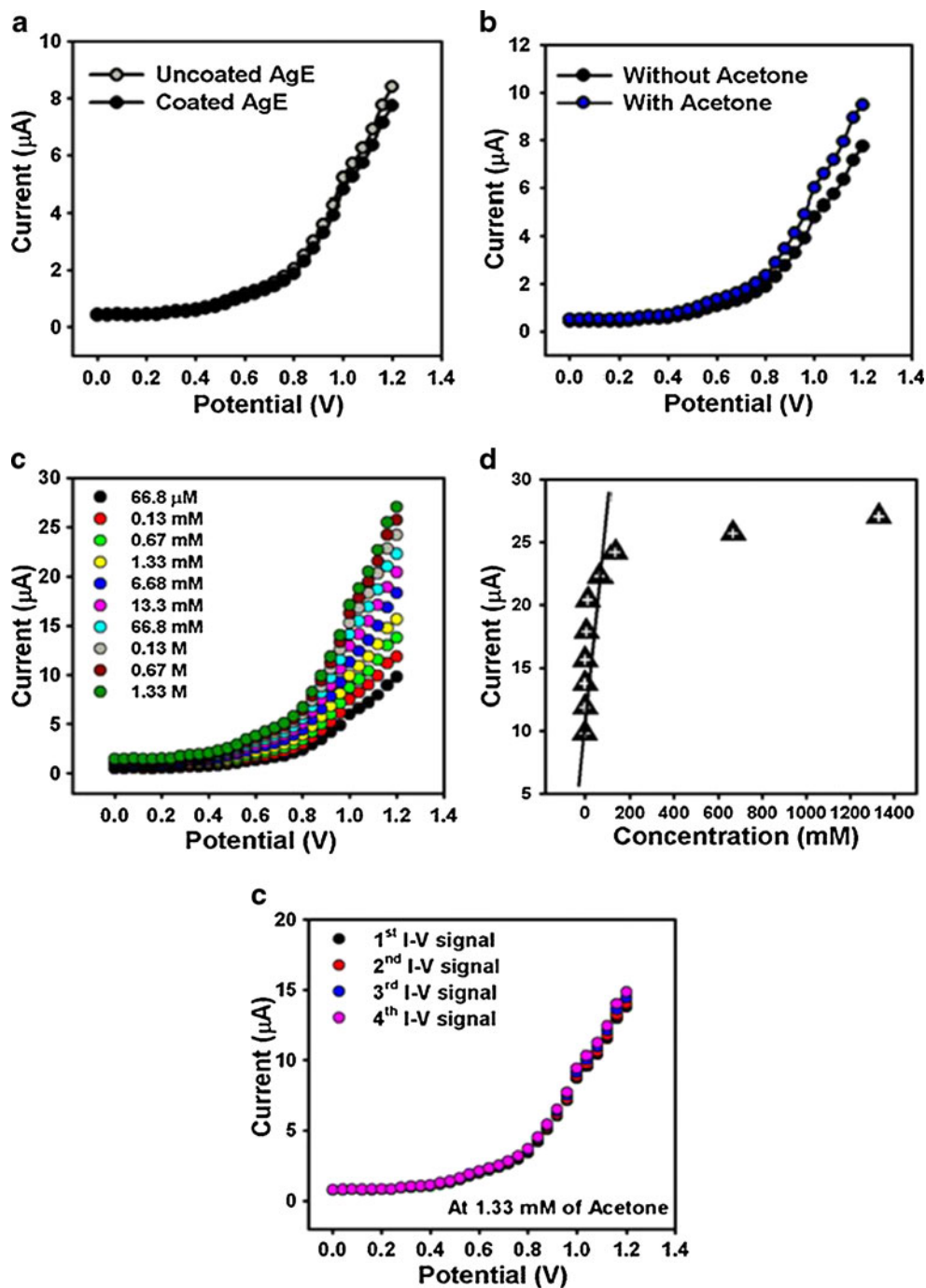surfaces. Potential was
between 0.0 and +1.2 V

Table 1 Comparison of the performances for acetone detection based on various material electrodes

Materials	LDR	Sensitivity	Detection limit	Linearity, r^2	Response time (s)	References
ZnO nanoparticles	0.13 mM to 0.13 M	0.14 μAcm^{-2} mM^{-1}	0.068±0.01 mM	–	10.0	[41]
Mn-ZnS QDs	1.0 to 600.0 mgL^{-1}	–	0.2 mgL^{-1}	–	–	[42]
Ag$_2$O microflowers	0.13 μM to 0.67 M	1.60 μAcm^{-2} mM^{-1}	0.11 μM	0.9462	10.0	[43]
Lead foil electrode	50 to 250 ppm	2.07 μAppm^{-1} cm^{-2}	50.0 ppm	0.9980	18.0	[44]
ZnO-Co$_3$O$_4$ nanorods	66.8 μM to 0.133 M	3.58 μAcm^{-2} mM^{-1}	14.7 μM	0.9684	10.0	Current work
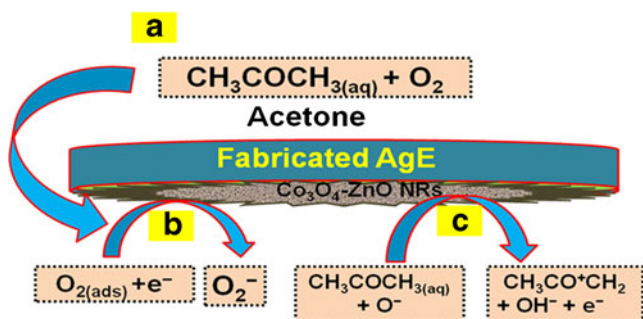
Scheme 2 Reaction mechanism of acetone on ZnO-doped Co$_3$O$_4$ NRs nanomaterial fabricated surfaces over AgE at room temperature. **a** Main reactive part of sensing reaction, **b** Reaction proceeded by adsorbing oxygen from reaction system (interior or exterior) in the initial step, **c** Reaction proceeded by releasing electrons to the reaction medium in the second step

the current reaches a saturated level which suggests that the active surface sites of NRs are saturated with acetone. The sensitivity is calculated from the calibration curve, which is close to 3.58 μAcm^{-2} mM^{-1}. The sensitivity value on the ZnO-doped Co$_3$O$_4$ NRs sensor is 25 times higher than on the previously reported un-doped ZnO nanostructure materials [41]. The linear dynamic range of this sensor ranges from 66.8 μM to 0.133 M (linearity, r^2=0.97), and the detection limit was calculated to be 14.7±0.2 μM [3 × noise (N)/slope(S)].

The response time for the ZnO-doped Co$_3$O$_4$ NRs coated-sensor to achieve a saturated steady state current was approximately 10.0 s. The prominent sensitivity of the sensor can be attributed to the good absorption (porous surfaces fabricated with binders) and adsorption ability, high catalytic activity, and good biocompatibility of the doped nanomaterials. Due to the large surface area, the nanomaterials displayed a beneficial nano-environment for acetone detection and recognition with excellent sensitivity (Scheme 1). The sensitivity of ZnO-doped Co$_3$O$_4$ NRs

affords high electron communication features which improved the direct electron movement between the active sites of NRs and the sensor electrode surfaces. Table 1 compares the analytical parameters for acetone sensors based on the performance of electrodes fabricated with various materials [41–44]. The modified thin ZnO-doped Co$_3$O$_4$ NRs sensor film exhibited better reliability and stability. However, due to the high dynamic surface area, the ZnO-doped Co$_3$O$_4$ NRs offered a productive environment for acetone adsorption and detection. The high sensitivity of NRs implies high electron-communication features which progress the direct electron communication between the active sites of ZnO-doped Co$_3$O$_4$ NRs and the sensor electrode [45]. To check the repeatability and storage stabilities, I-V response for the doped nanomaterial coated sensor was examined (up to 4 weeks), and the results are presented in Fig. 4e. After each experiment, the fabricated sensor was washed thoroughly with the phosphate buffer solution and no significant decrease on current responses was obtained. The sensitivity remained almost constant over a period of 4 weeks; after that the response of the fabricated sensor gradually decreases.

Redox reaction takes place on the surface of the semiconductor ZnO-doped Co$_3$O$_4$ NRs by reacting with the dissolved O$_2$ in bulk solution as well as with the surface-air of the neighboring atmosphere (interior or exterior). The acetone sensitivity towards ZnO-doped Co$_3$O$_4$ NRs could be attributed to the oxygen deficiency and enhance the oxygen adsorption on the surface of doped nanomaterials. The oxidation of acetone depends on the amount of adsorbed oxygen. If the adsorbed oxygen on the sensor surface is high, then the oxidizing potential with be higher be the oxidation of acetone will be fast [46]. When acetone reacts with negatively charged adsorbed oxygen, it oxidizes to small components, releasing free electrons (e$^-$) to the conduction band of ZnO-doped Co$_3$O$_4$ NRs, according to

Scheme 3 Reaction mechanism of acetone in the presence of semiconductor ZnO-doped Co$_3$O$_4$ NRs at room temperature **a** Oxygen adsorbed on the surrounding of nanomaterials in the reaction system, **b** Reduction of acetone by releasing electrons to enhance the sensitivity of fabricated sensors
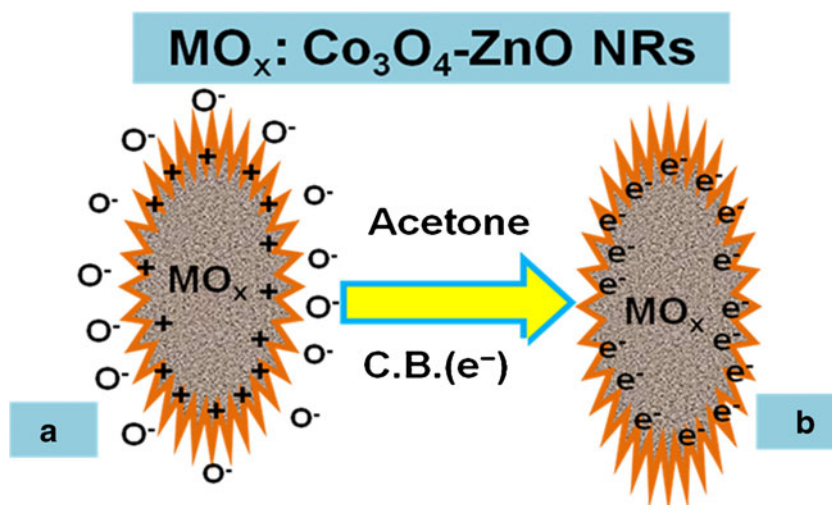
Scheme 2. Scheme 2 presents the main reactant (acetone & oxygen) in A, initial reaction of acetone with oxygen in B, secondary step of reaction proceeds by releasing electrons to the sensor surface in C.

The possible reaction could also be expressed by the following Scheme 3. Scheme 3a and b display the oxygen adsorbed on the surroundings of semiconductor doped nanomaterials in the reaction system and reduction of acetone by releasing electrons to enhance the sensitivity of fabricated sensors at room temperature respectively. These produced electrons contribute to a rapid increase in conductance of the fabricated thick-film of ZnO-doped Co_3O_4 NRs and hence enhance the sensitivity [47]. ZnO-doped Co_3O_4 NRs exhibit several approaches to providing chemical-based sensors and encouraging improvement has been accomplished in the research section. In spite of this development, there are still a number of important questions that are in need of additional investigation before this chemical sensor can be moved to commercial levels for established applications.

Conclusions

Finally, a sensor is fabricated using hydrothermally prepared ZnO-doped Co_3O_4 NRs with practically controlled shape structure, which exposed a constant morphological improvement in nanostructure materials and potential environmental applications. Semiconductor doped nanomaterials allow for a very sensitive transduction of the liquid/surface interactions for the chemical detections. This opportunity provides a variety of structural morphology assessments based on different approaches to the modification of the acetone molecules with metal oxide nanostructures. ZnO-doped Co_3O_4 NR is used to fabricate a simple and efficient chemical detection method consisting of side-polished AgEs and measuring the particular acetone detection at room temperature. To the best of our knowledge, this is the first report for highly sensitive detection of acetone with ZnO-doped Co_3O_4 NRs using simple and reliable I-V method in short response time. This approach has been described for the detection of acetone with doped nanomaterials and shows various attractive and potential features such as simplicity, reproducibly, rapidity, reliability, and inexpensiveness. We hope that this I-V method with semiconductor doped nanomaterials can be attractive for simultaneous detection of toxic chemicals in environmental and healthcare fields.

References

1. Chakraborti D, Narayan J, Prater JT (2007) Room temperature ferromagnetism in Zn1–xCuxO thin films. Appl Phys Lett 90:062504
2. Umar A, Rahman MM, Kim SH, Hahn YB (2008) Zinc oxide nanonail based chemical sensor for hydrazine detection. Chem Commun 166
3. Wang ZL (2004) Zinc oxide nanostructures: growth, properties and applications. J Phys Condens Matter 16:R829–R858
4. Ng HT, Han J, Yamada T, Nguyen P, Chen YP, Meyyappan M (2004) Single crystal nanowire vertical surround-gate field-effect transistor. Nano Lett 4:1247
5. Soci C, Zhang A, Xiang B, Dayeh SA, Aplin DPR, Park J, Bao XY, Lo YH, Wang D (2007) ZnO nanowire UV photodetectors with high internal gain. Nano Lett 7:1003
6. Li QH, Liang YX, Wan Q, Wang TH (2004) Oxygen sensing characteristics of individual ZnO nanowire transistors. Appl Phys Lett 85:6389–6391
7. Lee CJ, Lee TJ, Lyu SC, Zhang Y, Ruh H, Lee H (2002) Field emission from well-aligned zinc-oxide nanowires grown at low temperature. J Appl Phys Lett 81:3648–3650
8. Huang MH, Mao S, Feick H, Yan H, Wu Y, Kind H, Weber E, Russo R, Yang P (2001) Room temperature ultraviolet nanowire nanolasers. Science 292:1897–1899
9. Wang XD, Song JH, Liu J, Wang ZL (2007) Direct-current nanogenerator driven by ultrasonic waves. Science 316:102–105
10. Zhang Z, Yi JB, Ding J, Wong LM, Seng HL, Wang SJ, Tao JG, Li GP, Xing GZ, Sum TC, Huan CHA, Wu T (2008) Cu-doped ZnO nanoneedles and nanonails: morphological evolution and physical properties. J Phys Chem C 112:9579
11. Li YG, Tan B, Wu YY (2006) Freestanding mesoporous quasi-single-crystalline Co_3O_4 nanowire arrays. J Am Chem Soc 128:14258
12. Yu Y, Chen CH, Shui JL, Xie S (2005) Nickel-foam-supported reticular CoO-Li2O composite anode materials for lithium ion batteries. Angew Chem Int Ed 44:7085
13. Xu R, Wang J, Li Q, Sun G, Wang E, Li S, Gu J, Ju M (2009) Porous cobalt oxide nanorods: facile syntheses, optical property and application in lithium-ion batteries. J Solid State Chem 182:3177
14. Schmidt-Mende L, MacManus-Driscoll JL (2007) ZnO-nanostructures, defects, and devices. Mater Today 10:40
15. Ge CQ, Xie CS, Zeng DW, Cai SZ (2007) J Am Ceram Soc 90:3263
16. Rahman MM, Umar A, Sawada K (2009) Development of amperometric glucose biosensor based on glucose oxidase co-immobilized with multi-walled carbon nanotubes at low potential. Sensors Actuators B 137:327
17. Awschlom DD, Smyth JF, Grinstein G, DiVincenzo DP, Loss D (1992) Phys Rev Lett 68:3092
18. Callegari A, Tonti D, Chergui M (2003) Photochemically grown silver nanoparticles with wavelength-controlled size and shape. Nano Lett 3:1565
19. Lai T, Lai Y, Lee C, Shu Y, Wang C (2008) Microwave-assisted rapid fabrication of Co_3O_4 nanorods and application to the degradation of phenol. Catal Today 131:105
20. Ahmed J, Ahmad T, Ramanujachary KV, Lofland SE, Ganguli AK (2008) Development of a microemulsion-based process for synthesis of cobalt (Co) and cobalt oxide (Co_3O_4) nanoparticles from

submicrometer rods of cobalt oxalate. J Colloid Interface Sci 321:434–441

21. Jiu J, Ge Y, Li X, Nie L (2002) Preparation of Co$_3$O$_4$ nanoparticles by a polymer combustion route. Mater Lett 54:260

22. Niederberger M, Garnweitner G, Buha J, Polleux J, Ba J, Pinna N (2006) Nonaqueous synthesis of metal oxide nanoparticles: review and indium oxide as case study for the dependence of particle morphology on precursors and solvents. J Sol-Gel Sci Technol 40:259

23. Godish T (1991) Indoor air pollution control. Lewis Publishers, Chelsea

24. Fleischer M, Simon E, Rumpel E, Ulmer H, Harbeck M, Wandel M, Fietzek C, Weimar U, Meixner H (2002) Detection of volatile compounds correlated to human diseases through breath analysis with chemical sensors. Sensors Actuators B 83:245

25. Faisal M, Khan SB, Rahman MM, Jamal A, Umar A (2011) Ethanol chemi-sensor: evaluation of structural, optical and sensing properties of CuO nanosheets. Mater Lett 65:1400

26. Gonga H, Hu JQ, Wang JH, Ong CH, Zhu FR (2006) Nano-crystalline Cu-doped ZnO thin film gas sensor for CO. Sensors Actuators B Chem 115:247

27. Francesco FD, Fuoco R, Trivella MG, Ceccarini A (2005) Breath analysis: trends in techniques and clinical applications. Microchim J 79:405

28. Nicoletti S, Zampolli S, Elmi I, Dori L, Severi M (2003) IEEE Sensors J 3:454

29. Aguilar-Leyva J, Maldonado A, De-la-Olvera M (2007) Gas-sensing characteristics of undoped-SnO$_2$ thin films and Ag/SnO$_2$ and SnO$_2$/Ag structures in a propane atmosphere. Mater Charact 58:740

30. Strom JGJ, Jun HW (1980) Kinetics of hydrolysis of methenamine. J Pharm Sci 69:1261

31. Wang RC, Lin HY (2011) Cu doped ZnO nanoparticle sheets. Mater Chem Phys 125:263

32. Laudise RA, Ballman AA (1960) Hydrothermal synthesis of zinc oxide and zinc sulphide. J Phys Chem 64:688

33. Dodd A, McKinley A, Tsuzuki T, Saunders M (2009) Tailoring the photocatalytic activity of nanoparticulate zinc oxide by transition metal oxide doping. Mater Chem Phys 114:382–386

34. Palard M, Balencie J, Maguer A, Hochepied JF (2010) Effect of hydrothermal ripening on the photoluminescence properties of pure and doped cerium oxide nanoparticles. Mater Chem Phys 120:79

35. Chu X, Zhang H (2009) Catalytic decomposition of formaldehyde on nanometer manganese dioxide. Mod Appl Sci 3:177

36. Rubio-Marcos F, Calvino-Casilda V, Banares MA, Fernandez JF (2010) Novel hierarchical Co$_3$O$_4$/ZnO mixtures by dry nanodispersion and their catalytic application in the carbonylation of glycerol. J Catal 275:288

37. Peiteado M, Makovec D, Villegas M, Caballero AC (2008) Influence of crystal structure on the CoII diffusion behavior in the Zn$_{1-x}$Co$_x$O system. J Solid State Chem 181:2456

38. Tak Y, Yong K (2008) A novel heterostructure of Co3O4/ZnO nanowire array fabricated by photochemical coating method. J Phys Chem C 112:74

39. Lupan O, Emelchenko GA, Ursaki VV, Chai G, Redkin AN, Gruzintsev AN, Tiginyanu IM, Chow L, Ono LK, Cuenya BR, Heinrich H, Yakimov EE (2010) Synthesis and characterization of ZnO nanowires for nanosensor applications. Mater Res Bull 45:1026

40. Rahman MM, Jamal A, Khan SB, Faisal M, Rub MA, Al-Youbi AO, Asiri AM (2012) Electrochemical determination of olmesartan medoxomil using hydrothermally prepared nanoparticles composed SnO$_2$–Co$_3$O$_4$ nanocubes in tablet dosage forms. Talanta 99:924

41. Khan SB, Faisal M, Rahman MM, Jamal A (2011) Low-temperature growth of ZnO nanoparticles: photocatalyst and acetone sensor. Talanta 85:943

42. Sotelo-Gonzalez E, Fernandez-Arguelles MT, Costa-Fernandez JM, Sanz-medel A (2012) Mn-doped ZnS quantum dots for the determination of acetone by phosphorescence attenuation. Anal Chem Acta 712:120

43. Rahman MM, Jamal A, Khan SB, Faisal M, Asiri AM (2011) Fabrication of highly sensitive acetone sensor based on sonochemically prepared as-grown Ag$_2$O nanostructures. Chem Eng J 192:122

44. Wang CC, Weng YC, Chou TC (2007) Acetone sensor using lead foil as working electrode. Sensors Actuators B 122:591

45. Rahman MM, Jamal A, Khan SB, Faisal M (2011) Fabrication of chloroform sensor based on hydrothermally prepared low-dimensional β-Fe$_2$O$_3$ nanoparticles. Superlattice Microst 50:369

46. Righettoni M, Tricoli A, Pratsinis SE (2010) Si:WO$_3$ sensors for highly selective detection of acetone for easy diagnosis of diabetes by breath analysis. Anal Chem 82:3581

47. Faisal M, Khan SB, Rahman MM, Jamal A, Asiri AM, Abdullah MM (2011) Smart chemical sensor and active photo-catalyst for environmental pollutants. Chem Eng J 173:178–184